DALTON PERSPECTIVE

Metal-containing carbon clusters †

Konstantin B. Shelimov, David E. Clemmer and Martin F. Jarrold

Department of Chemistry, Northwestern University, 2145 Sheridan Road, Evanston, IL 60208, USA

The results of injected-ion drift-tube studies of the structures and isomerization of metal-containing carbon clusters are described. Three basic types of geometry are observed: metal-containing rings, metal-containing graphitic fragments and metallofullerenes. The nature of these isomers depends on the electronic properties of the metal. While only a few metals and stoichiometries have been examined so far, it is possible to begin to identify periodic trends in both the structures and properties.

If a piece of bulk material is made smaller and smaller its properties ultimately change. The electronic properties are generally the first to be modified. For example, quantum confinement effects increase the band gap in semiconductor particles with dimensions as large as 100–1000 Å.[1] At smaller dimensions, around 10–100 Å, the number of surface atoms becomes a significant fraction of the number of atoms in the cluster. In this size regime the geometry may depart from that of the bulk crystal structure. Metal clusters, for example, may adopt icosahedral packing, which cannot exist in an extended lattice. For even smaller clusters, with less than around 100 atoms, the properties can change dramatically with the addition or removal of only a single atom. For example, the physical and chemical properties of naked free-electron metal clusters change abruptly due to electronic shell closings.[2] Unusual and unexpected geometries may also exist in this size regime, possibly only for some special clusters with a particular 'magic' number of atoms. The fullerenes are a good example.[3] They are more stable than small graphite fragments, because it is energetically favourable to tie up the dangling bonds at the edges of such a fragment by incorporating pentagons and generating a spheroidal geometry.

While a wide variety of physical and chemical properties can be probed, probably the single most important piece of information for clusters in the small size regime is their structure. However, obtaining such structural information has been difficult. This is partly because it is not possible, except in a few special cases, to produce macroscopic amounts of a cluster containing a particular number of atoms. Furthermore, naked clusters are often highly reactive, which means that they must be prepared and studied in carefully controlled environments, such as in the gas phase or in an inert matrix. These factors preclude the use of the wide range of analytical techniques usually available to chemists. Spectroscopic techniques for studying species in the gas phase, such as resonant two-photon ionization, have had limited success, except for the smallest clusters, and matrix studies have been hindered by the difficulty in preparing a monodisperse cluster sample. As a result of these limitations, detailed spectroscopic information is available for only a handful of clusters with more than four atoms. Furthermore, the methods employed to date are not easily extended, in practice, to significantly larger clusters (> 20 atoms), particularly when a variety of structural isomers are present. Because of these problems, structural information is often deduced indirectly from, for example, 'magic' numbers in mass spectra, chemical reactivity patterns and fragmentation behaviour. An alternative, and really completely different approach, is to passify the surface of the cluster with ligands. While this has the advantage that macroscopic amounts may be generated and manipulated under ordinary conditions, passification must affect the geometries and properties of the clusters.

In this article we will describe recent efforts to obtain structural information for metal-containing carbon clusters. These clusters have recently received a considerable amount of attention. A remarkably wide variety of stoichiometries and geometries is possible. For example, exohedral and endohedral metallofullerenes have been generated, some of which have been prepared in bulk quantities.[4] Metallocarbohedranes, clusters with the general formula M_8C_{12}, have been found to form for the early transition metals, though these have not yet been prepared in macroscopic amounts.[5] In addition, metal carbide nanocrystals have been observed in gas-phase experiments.[6] Given these results, it seems reasonable to expect that novel geometries may exist for other metal-containing carbon clusters, and it is possible that some of these could be prepared in macroscopic amounts, leading to new materials. In the work described here, we have attempted to perform a systematic study of metal-containing carbon clusters, first considering a variety of clusters containing a single metal atom, before proceeding to clusters with multiple metal atoms.

Information about the geometries of the metal-containing carbon clusters has been obtained from ion-mobility measurements.[7] The mobility of a gas-phase ion is a measure of how rapidly it moves through an inert buffer gas under the influence of a weak electric field. It depends on the ion's average collision cross-section, which in turn depends on its geometry. The use of ion-mobility measurements to resolve structural isomers of gas-phase ions was first demonstrated close to twenty years ago, but it is only in the last five years that this approach has been exploited to deduce structural information. Structural information is obtained from the ion-mobility measurements by comparing the measured mobilities to mobilities calculated from orientationally averaged collision cross-sections for assumed geometries.[8] This approach cannot provide detailed structural information such as the precise location of all the atoms in the clusters, but it can be used to resolve different families of isomers.[9] The spectroscopic information required for precise structural determination is not easy to obtain, particularly for a wide range of different clusters.

Experimental Methods

A schematic diagram of the injected-ion drift-tube apparatus used in the studies described here is shown in Fig. 1.[10] Cluster ions are generated by pulsed laser vaporization of a metal-

† Basis of the presentation given at Dalton Discussion No. 1, 3rd–5th January 1996, University of Southampton, UK.

Non-SI units employed: Torr ≈ 133 Pa, eV ≈ 1.60 × 10^{-19} J.

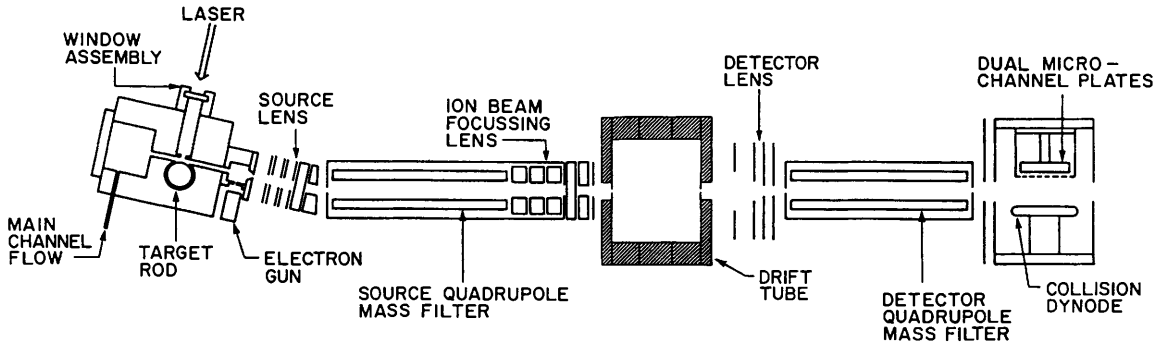

Fig. 1 Schematic diagram of the injected-ion drift-tube apparatus

doped graphite rod in a continuous flow of helium buffer gas. After exiting the source, the cluster ions are focussed into a quadrupole mass-spectrometer where a particular $M_mC_n^+$ cluster is mass-selected. The mass-selected clusters are then focussed into a low-energy ion beam and injected into the drift tube. The drift tube contains helium buffer gas at a pressure of around 5 Torr, and there is a drift field of 13.12 V cm^{-1} across its length. Ions travel across the drift tube under the influence of the electric field, and some exit through a small aperture. The exiting ions are focussed into a second quadrupole mass spectrometer, and then detected. The second quadrupole mass spectrometer is employed in studies of the fragmentation or chemical reactivity of the clusters in the drift tube. To measure mobilities, 50 μs pulses of mass-selected clusters are injected into the drift tube, and their arrival-time distribution is recorded at the detector with a multichannel scaler. The arrival-time distribution is converted into a drift-time distribution by correcting the time-scale to reflect the amount of time it takes for the ions to travel across the drift tube.

LaC_n^+ clusters

Fig. 2 shows drift-time distributions recorded for LaC_6^+, LaC_{16}^+, LaC_{26}^+, LaC_{36}^+ and LaC_{46}^+.[11] There is a number of clearly resolved peaks in these distributions resulting from structural isomers with different average collision cross-sections. Isomers with larger cross-sections occur at longer times in the distributions because they move more slowly across the drift tube. As will be described below, the peaks present in Fig. 2 can be assigned to specific geometries. Briefly, the assignments are: metallofullerene (labelled full); graphite fragment (gr); bicyclic rings (ring II) and monocyclic rings (ring Ia and ring Ib). The monocyclic rings dominate for the small clusters. Ring Ia generally dominates for clusters with an even number of carbon atoms, while ring Ib generally dominates for the odd-numbered ones. Ring II emerges at around 20 carbon atoms, and the graphite fragment, gr, emerges at around 26 carbon atoms. The fullerene first appears around 29 carbon atoms, and dominates the isomer distribution for clusters with more than 40 carbon atoms.

Fig. 3 shows a plot of the inverse mobilities of all the features observed in the drift-time distributions for LaC_n^+ clusters with up to 90 carbon atoms.[11] The mobilities were obtained from equation (1) where t_D is the drift time, L is the length of the drift

$$K_o = \frac{L}{t_D E} \cdot \frac{P}{760} \cdot \frac{273.2}{T} \qquad (1)$$

tube, E is the electric field, P is the buffer gas pressure in Torr and T is the temperature in K. The inverse mobilities plotted in Fig. 3 are proportional to the average collision cross-section. The different families of isomers, labelled ring Ia, ring Ib, ring II, graphite and fullerene, are apparent in the figure. These have been assigned to specific geometries by comparison with

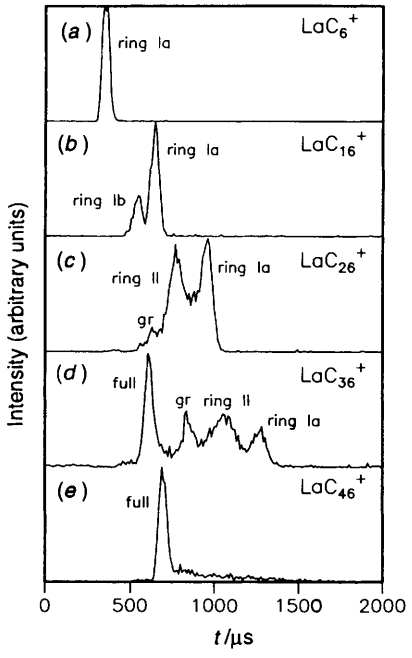

Fig. 2 Drift-time distributions recorded for LaC_6^+, LaC_{16}^+, LaC_{26}^+, LaC_{36}^+ and LaC_{46}^+ with an injection energy of 50 eV. Almost no isomerization or dissociation occurs with this injection energy, so that the drift-time distributions reflect the isomer distributions coming from the source. The geometries observed are the three ring isomers (labelled ring Ia, ring Ib and ring II), metal-containing graphite fragments (gr), and metallofullerenes (full)

previous measurements for pure carbon clusters,[9,12] and by comparing the measured mobilities to mobilities calculated for assumed geometries. For example, the LaC_n^+ isomers labelled fullerene can be assigned to metallofullerenes because they have almost the same inverse mobility as those of the pure carbon fullerenes (shown by the solid line in the figure). The close agreement between the inverse mobilities of the LaC_n^+ fullerenes and of the pure carbon fullerenes suggests that the metal atom is in an endohedral position. The inverse mobilities are expected to be around 10% larger if the metal is outside of the cage. As can be seen from Fig. 3 the inverse mobilities of the LaC_n^+ fullerenes abruptly increase for clusters with less than 38 carbon atoms. This increase is attributed to the metal atom moving to a non-endohedral position because the cage has become too small to accommodate it. A similar analysis for the graphite fragment suggests that it is roughly circular, and near-planar, with the metal atom attached to the edge, rather than sitting on top.

While fullerenes dominate the isomer distributions for the larger LaC_n^+ clusters, the ring isomers are dominant for the smaller ones ($n < 30$). A variety of ring isomers have also been observed for pure carbon clusters in this size regime. The

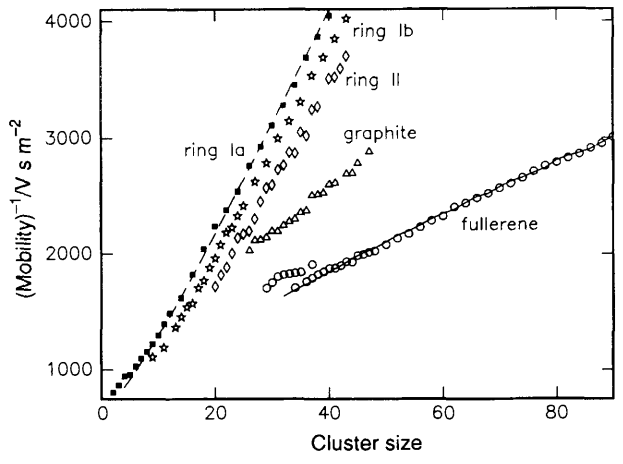

Fig. 3 Plots of the inverse mobilities of the observed LaC_n^+ isomers against cluster size. The line shows the inverse mobilities of pure carbon fullerenes. The dashed line shows calculated inverse mobilities for a LaC_n^+ monocyclic ring isomer where the metal atom is part of the ring

families of LaC_n^+ isomers labelled ring Ia, ring Ib and ring II have inverse mobilities that are similar to the inverse mobilities of the pure carbon rings. More information about the geometries of these families of isomers can be obtained by comparing the measured mobilities to those calculated for assumed geometries. Mobilities are calculated from equation (2).[13] In this expression m and m_B are the masses of the cluster

$$K = \frac{(18\pi)^{\frac{1}{2}}}{16}\left(\frac{1}{m}+\frac{1}{m_B}\right)^{\frac{1}{2}}\frac{e}{(k_BT)^{\frac{1}{2}}}\cdot\frac{1}{Q}\cdot\frac{1}{N} \qquad (2)$$

and buffer gas, N is the buffer gas number density, and Q is the orientationally averaged collision cross-section obtained from equation (3) where $q(\theta, \varphi)$ is the collision cross-section for a

$$Q = \int_0^{\pi} d\theta \cos\theta \int_0^{2\pi} d\varphi\, q(\theta, \varphi) \qquad (3)$$

collision geometry defined by θ and φ. By comparison of the measured mobilities to those calculated for assumed geometries: ring Ia is assigned to a monocyclic ring where the lanthanum is part of the ring; ring Ib is attributed to a monocyclic carbon ring with the lanthanum sitting inside the ring and ring II is assigned to bicyclic rings generated by coalescence of LaC_n^+ rings with pure carbon rings. The dashed line in Fig. 3 shows calculated inverse mobilities for the monocyclic ring isomer where the metal atom is part of the ring. The calculated inverse mobilities are in good agreement with inverse mobilities for the ring Ia family of isomers over the entire size range. Other geometries may have mobilities which fit at least some of the experimental data, however the geometries described above are believed to be the most plausible assignments.

It is worth briefly considering the bonding in the ring isomers.[14] For pure carbon rings, cumulene (=C=C=C=) and polyacetylene (–C≡C–C≡C–) bonding schemes have similar energies.[15] Since the ionization energy for lanthanum is significantly less than the ionization energy of the carbon fragment, the charge will be localized on the metal leaving a formally divalent lanthanum. If the divalent La^+ is inserted into a carbon ring it drives the rest of the ring to adopt a polyacetylene bonding scheme, which can only propagate around the ring for an even number of carbon atoms. This probably accounts for why the ring Ia isomers generally dominate for clusters with an even number of atoms. On the other hand, a geometry where the metal atom sits inside the ring is expected to be more favourable for clusters with an odd number of carbon atoms. This geometry can be stabilized by ionic interactions (similar to those believed to be responsible for the stability of endohedral metallofullerenes). Charge transfer from the metal atom to the ring is more favourable for the odd-numbered rings because they have larger electron affinities.[16] Thus the geometry where the metal atom sits inside the ring should be more favourable for odd-numbered clusters.

The studies described above have focussed on clusters that come directly from the source. A laser vaporization source provides a non-equilibrium environment for cluster growth and may not yield the lowest-energy structural isomers. To determine if the clusters are in their lowest-energy geometry it is necessary to anneal them. This can be accomplished by injecting them into the drift tube at elevated kinetic energies. As the ions enter the drift tube they undergo collisions with the buffer gas atoms, which convert some of the cluster's kinetic energy into internal energy. The cluster's kinetic energy is thermalized, and further collisions with the buffer gas then cool the hot clusters. Thus the clusters experience a transient heating cycle as they enter the drift tube, and while they are hot they may isomerize. At high injection energies the clusters may be heated to the point where they fragment. The transient heating cycle occurs very close to the entrance of the drift tube, so the rest of the drift tube can be used to probe the geometries of the annealed clusters or fragments. Fig. 4 shows the effects of increasing the injection energy and annealing LaC_{26}^+ and LaC_{36}^+. For LaC_{26}^+ two ring isomers, ring Ia and ring II, are present at low injection energies [40 eV in Fig. 4(*a*)]. As the injection energy is raised [140 eV in Fig. 4(*b*)] nearly all of the ring II isomer disappears. Since little fragmentation is observed at the injection energies used to record the data shown in the figure, ring II must have isomerized into ring Ia. Conversion of ring II into Ia is an isomerization process that is relatively easy to understand. Ring II has been attributed to a bicyclic ring. The rings are highly strained because the bond angles of the sp^1 carbon atoms in the rings are bent away from 180°. Isomerization from a bicyclic ring to a monocyclic ring reduces the strain energy. An analogous isomerization process is observed for LaC_n^+ clusters with an odd number of carbon atoms, except here the ring II isomers anneal into ring Ib instead of ring Ia.

Drift-time distributions for LaC_{36}^+, recorded with injection energies of 50 and 225 eV, are shown in Fig. 4. At the lower injection energy [Fig. 4(*c*)] four isomers are present: the fullerene, graphite fragment, and two ring isomers, ring II and ring Ia. At the higher injection energy, the ring isomers have almost all disappeared. Only a small amount of fragmentation is observed, so most of the ring isomers must have converted into the graphite fragment and fullerene. Isomerization of pure carbon rings into fullerenes has also been observed. Indeed, the mechanism of fullerene synthesis is now believed to involve coalescence of carbon rings followed by isomerization to the fullerene geometry.[17] However, isomerization of pure carbon rings into graphite fragments has not been observed. The graphite fragment is not an important isomer for pure carbon clusters; it never amounts to more than a few percent of the isomer distribution.[12] Another important difference between the pure carbon clusters and LaC_n^+ clusters is the efficiency of fullerene formation. Fullerene formation is inefficient for C_{36}^+ (most of the C_{36}^+ rings fragment rather than form a fullerene), while for LaC_{36}^+ over 60% of the rings convert into a fullerene. So the presence of the lanthanum atom promotes fullerene formation. This enhancement probably occurs by the lanthanum atom relieving the strain energy that builds up during the early stages of the isomerization process (the low ionization energy of lanthanum may also promote isomerization by influencing the energetics of the isomers involved). Isomerization of LaC_n^+ rings into graphite fragments only occurs over a narrow range of cluster sizes, from around 28 to 37 carbon atoms. This is the size regime where fullerenes

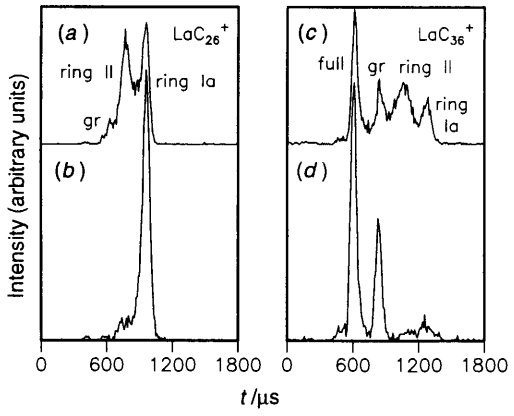

Fig. 4 Drift-time distributions for LaC_{26}^+ at injection energies of (*a*) 40 and (*b*) 140 eV and for LaC_{36}^+ at injection energies of (*c*) 50 and (*d*) 225 eV

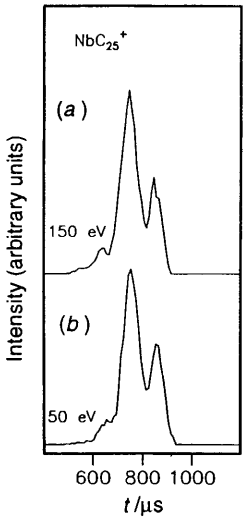

Fig. 5 Drift-time distributions for NbC_{25}^+ at injection energies of (*a*) 50 and (*b*) 150 eV

emerge. Small fullerenes are highly strained and the graphite fragment is presumably energetically competitive. For slightly larger clusters the strain energy decreases, and the fullerene dominates.

The results presented above provide some important clues about how the metal-containing carbon clusters are assembled. For example, the shift from monocyclic rings to bicyclic rings with increasing cluster size suggests that the medium-sized clusters grow by coalescence of smaller rings. A similar process has been suggested to occur for pure carbon clusters. The annealing studies show that once the LaC_n^+ rings reach a critical size of slightly more than 30 atoms, they can isomerize into fullerenes. This isomerization process generates endohedral metallofullerenes (when the metal fits) with remarkably high efficiency (> 90% for LaC_{60}^+)[18]

NbC_n^+ clusters

The isomers observed for NbC_n^+ clusters are similar to those observed for LaC_n^+.[19] Ring isomers dominate for the smaller clusters, while the fullerene dominates for the larger ones. There are, however, significant differences between the NbC_n^+ and LaC_n^+ clusters which can be traced to the different chemical properties of the metal. First, the apparent analogue of the LaC_n^+ ring Ia isomer is abundant for NbC_n^+ clusters with both an odd and even number of carbon atoms, while for LaC_n^+ this isomer is much more abundant for clusters with an even number of carbon atoms. Assuming that the charge is localized on the metal, the Nb^+ is tetravalent, in contrast to La^+, which is divalent. Thus when the Nb^+ inserts into a carbon ring it can essentially substitute for a carbon atom, and this isomer is stable for both odd- and even-numbered clusters.

The NbC_n^+ monocyclic rings are only observed for clusters containing up to around 25 carbon atoms, where the bicyclic rings quickly become dominant. For LaC_n^+ clusters the monocyclic ring persists to much larger cluster sizes. As described above, the LaC_n^+ bicyclic rings isomerize to monocyclic rings. The results of annealing studies for NbC_{25}^+ are shown in Fig. 5. The NbC_{25}^+ bicyclic ring persists to high injection energies; it apparently does not anneal into a monocyclic ring. This provides a rationale for why the monocyclic ring is only observed for relatively small NbC_n^+ clusters, while for LaC_n^+ clusters, where the bicyclic rings anneal into monocyclic rings, the latter are observed for larger cluster sizes. This difference clearly must be related to the different chemical properties of the metal. When a divalent La^+ is inserted or attached to a carbon ring its two valence electrons are involved in bonding and there is insufficient valence-electron density available to activate a C–C bond or form an additional strong La–C bond. Thus when a LaC_n^+ monocyclic ring interacts with a carbon ring to form a bicyclic ring the linkage probably occurs through carbon–carbon bonds. For pure carbon rings this interaction is believed to occur through a [2 + 2] cycloaddition to yield a bicyclic ring that can convert into a monocyclic ring by a perpendicular retro [2 + 2] addition. The presence of the lanthanum does not appear to affect the ring-opening process. On the other hand, a Nb^+ that is either inserted or attached to a carbon ring has sufficient valence-electron density to activate carbon–carbon bonds and form additional strong metal–carbon bonds. So, if an NbC_n^+ ring interacts with a carbon ring the linkage can occur through the niobium atom leading to a bicyclic ring with the niobium at the junction between the two rings. The niobium atom in this position may inhibit isomerization to a monocyclic ring.

Another significant difference between the NbC_n^+ and LaC_n^+ clusters occurs with the metallofullerene isomer. Fig. 6 shows a plot of the inverse mobilities of the fullerene isomer for C_n^+, LaC_n^+ and NbC_n^+ clusters.[20] The larger LaC_n^+ fullerenes have inverse mobilities that are similar to those of the pure carbon fullerenes, indicating that the metal is endohedral. For LaC_n^+ fullerenes with less than around 38 carbon atoms the inverse mobilities increase abruptly as the cage becomes too small to accommodate the metal atom. For small NbC_n^+ fullerenes the cage is also too small to accommodate a niobium atom, and the inverse mobilities are similar to the inverse mobilities of the smaller LaC_n^+ clusters. The inverse mobilities of some of the NbC_n^+ metallofullerenes decrease for clusters with more than around 36 carbon atoms; this is the size regime where the cage becomes large enough to accommodate the niobium atom. However, there are substantial oscillations in the inverse mobilities of the larger NbC_n^+ fullerenes. It appears that fullerenes with an even number of carbon atoms have an endohedral metal atom while the odd-numbered ones are non-endohedral.

Pure carbon fullerenes with an odd number of carbon atoms are much less abundant than the even-numbered ones, which indicates that the former are much less stable. Because of topological constraints, a closed-cage fullerene can only form for an even number of carbon atoms, and odd-numbered fullerenes have a defect due to the missing carbon atom. For the NbC_n^+ fullerenes, however, the odd- and even-numbered ones have comparable abundances. This indicates that the NbC_n^+ fullerenes with an odd number of carbon atoms are relatively stable. It seems likely that in the larger non-endohedral NbC_n^+ fullerenes the metal atom occupies the defect site in the fullerene cage, where it stabilizes the odd-numbered fullerenes. Since the metal atom is part of the carbon network in this geometry we refer to it as a networked metallofullerene. Fig. 7 shows a diagram of a NbC_{35} networked metallofullerene. The niobium–

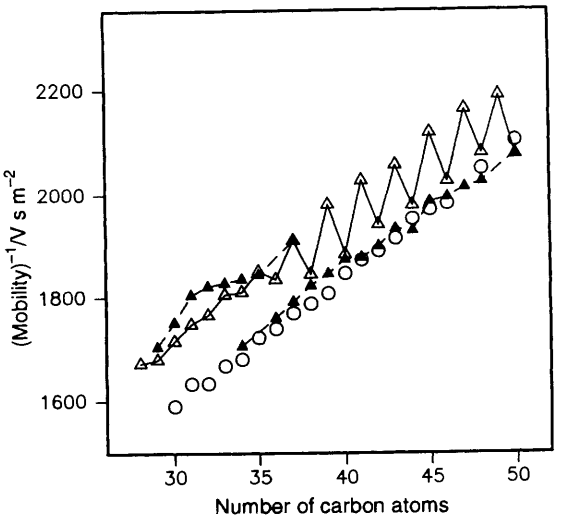

Fig. 6 Plots of the inverse mobilities of the fullerene isomers for C_n^+ clusters (○), LaC_n^+ clusters (▲) and NbC_n^+ clusters (△)

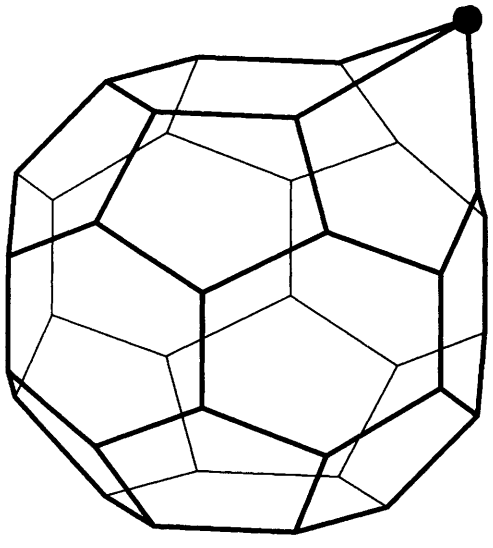

Fig. 7 Schematic diagram of a networked metallofullerene geometry for NbC_{35}. This geometry is obtained by replacing a carbon atom in C_{36} fullerene by a niobium atom

carbon bonds are longer than carbon–carbon bonds and so the metal protrudes from the surface of the carbon cage. For this reason, the calculated inverse mobilities of the networked isomer are almost identical to those for the exohedral geometry (where the metal atom is bound to the outside of the fullerene cage).

There are indications that the networked metallofullerene geometry also exists for some LaC_n^+ clusters. As can be seen from Fig. 6, as the cage shrinks LaC_{37}^+ is the first lanthanum-containing fullerene to have a non-endohedral geometry. However, LaC_{36}^+ is endohedral; LaC_{35}^+ is non-endohedral and both endohedral and non-endohedral geometries are present for LaC_{34}^+. Clearly, the position of the metal atom oscillates in this size regime, and it moves out of the cage preferentially for the LaC_n^+ clusters with an odd number of carbon atoms. This presumably occurs because the metal atom can occupy the defect site in the odd-numbered fullerene. The relative abundances of the odd-numbered LaC_n^+ fullerenes are larger than those of the even-numbered ones in this size regime, indicating that the networked metal atom stabilizes the odd-numbered fullerenes.

While the networked isomer forms for LaC_n^+ fullerenes in the size regime where the cage becomes too small to accommodate the metal atom, it forms for all of the larger odd-numbered NbC_n^+ fullerenes. This difference can be traced to the different electronic properties of the metal atom. Both theoretical[21] and experimental studies[4] have indicated that there is a large ionic contribution to the stability of endohedral metallofullerenes. Lanthanum has three valence electrons and relatively low ionization energies so that charge transfer from the metal to the carbon cage and formation of the endohedral geometry (which maximizes electrostatic interactions) is favourable. On the other hand, niobium has five valence electrons and relatively high ionization energies. Thus charge transfer and ionic bonding are less favourable. Because the niobium atom retains more of its electron density, however, it can readily form localized covalent bonds at the defect site of odd-numbered fullerenes, to produce a stable networked geometry.

Endohedral metallofullerenes, however, do form for large NbC_n^+ clusters with an even number of carbon atoms. This can be understood in terms of the energetic differences between C–C and M–C covalent bonds. The bond energies of even the strongest M–C single and double bonds ($\approx$2.5 and $\approx$4.1 eV, respectively)[22] are smaller than those of C–C single and double bonds ($\approx$3.8 and 7.5 eV, respectively).[23] Thus while the ionic interactions discussed above are probably weaker for niobium, the large energy difference between forming C–C and Nb–C bonds favours the all-carbon cage, rather than the metal-substituted cage, for NbC_n^+ fullerenes with an even number of carbon atoms.

Based on the preceding discussion we expect that networked metallofullerenes will most likely form for metals in Groups 4 (Ti, Zr and Hf), 5 (V, Nb and Ta) and possibly 6 (Cr, Mo and W). The first and second ionization energies of these metals are significantly higher than those for lanthanum and most of the other metals that are thought to form endohedral metallofullerenes.[24] Networked metallofullerenes have recently been observed for some ZrC_n^+ clusters.[25]

PdC_n^+ clusters

The data discussed above, along with theoretical calculations and periodic trend considerations,[24] suggest that the overriding factor that influences endohedral metallofullerene formation is the ability of the metal to transfer electron density to the carbon cage. The endohedral geometry maximizes ionic interactions between the positively charged metal and the negatively charged cage. A competing geometry, the networked metallofullerene, results when the metal retains sufficient electron density to bond covalently into the cage. For these reasons, early transition metals, such as scandium, yttrium and lanthanum, form endohedral metallofullerenes, while metals in the middle of the Periodic Table (such as niobium and zirconium) can also form networked structures. The question of what happens with transition metals on the right-hand side of the Periodic Table quickly arises. As one moves to the right side of the Periodic Table the d orbitals fill up and contract. So one might expect that these metals will behave differently from either the early or middle transition metals. To determine what isomers are present for the late transition metals, PdC_n^+ clusters were studied.[26]

The drift-time distribution recorded for PdC_{33}^+, with an injection energy of 50 eV, is shown in the insert in Fig. 8. The shaded area is attributed to $Pd_2C_{24}^+$, which is impossible to separate from PdC_{33}^+ because of palladium's broad isotope distribution. The inverse mobilities of the isomers observed for PdC_n^+ (n = 10–43) clusters are plotted in Fig. 8. There are three families of isomers. Comparison of the inverse mobilities for these isomers with those measured for C_n^+ and MC_n^+ (M = La or Nb) clusters indicates that the PdC_n^+ isomers are metal-containing monocyclic rings, bicyclic rings and graphite fragments. The PdC_n^+ monocyclic rings dominate the unannealed isomer distributions for clusters with fewer than

30–35 carbon atoms (the metal is either inserted into or attached to the outside of these rings), and bicyclic rings dominate for larger clusters. The graphite fragment is a minor isomer ($\approx$15%) for the larger clusters. Fullerenes are not a significant isomer for any of the PdC_n^+ clusters.

As described above, bicyclic C_n^+ and LaC_n^+ rings isomerize into monocyclic rings when the injection energy is raised, while NbC_n^+ bicyclic rings do not isomerize in this way. Annealing studies of PdC_n^+ clusters show that bicyclic rings with an odd number of carbon atoms isomerize into monocyclic rings, while those with an even number do not isomerize. This behaviour explains why the bicyclic rings are more abundant in the unannealed isomer distributions for clusters with an even number of carbon atoms. However, it is not clear at present why the odd- and even-numbered PdC_n^+ clusters behave so differently.

The MC_n^+ (M = La or Nb) rings with more than around 30 carbon atoms isomerize into fullerenes and graphite fragments when collisionally annealed. We have used the same approach in an effort to produce Pd-containing fullerenes. However, collisional heating of PdC_n^+ clusters leads to their complete dissociation through the loss of a palladium atom at injection energies similar to those normally required for efficient fullerene formation. Fig. 9 shows drift-time distributions recorded for the C_{50}^+ product resulting from injection of PdC_{50}^+ clusters into the drift tube at energies of 120 and 200 eV. At 120 eV around 10% of the PdC_{50}^+ clusters fragment to give C_{50}^+. The products are predominantly fullerenes, with small amounts of graphite fragments and monocyclic rings. Since there are no fullerene isomers present for the PdC_{50}^+ precursor, the most likely explanation for these results is that the loss of the palladium atom is driven by the exothermicity released during isomerization of the ring isomers to the fullerene. At 200 eV more than 90% of the injected PdC_{50}^+ clusters fragment to give C_{50}^+. Fig. 9 shows that it is mainly fullerene, though a significant amount of monocyclic ring is also present.

In view of the previous unsuccessful attempts to prepare macroscopic amounts of metallofullerenes of late transition metals, the absence of the endohedral isomer in these experiments is not a surprise. The endohedral isomer is presumably not very stable because ionic interactions are not favourable for high-ionization-energy metals like palladium. On the other hand formation of a networked metallofullerene presumably requires the ability to form strong metal–carbon bonds. The measured $(La–CH_3)^+$ [27] and $(Pd–CH_3)^+$ [28] bond energies are similar. Therefore the much higher stability of

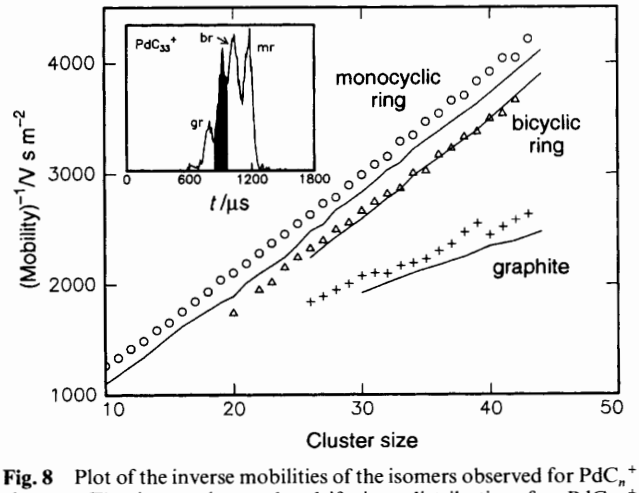

Fig. 8 Plot of the inverse mobilities of the isomers observed for PdC_n^+ clusters. The insert shows the drift-time distribution for PdC_{33}^+ recorded with an injection energy of 50 eV (mr = monocyclic ring, br = bicyclic ring, gr = graphite fragment). The shaded peak is believed to be due to a $Pd_2C_{24}^+$ contaminant

LaC_n^+ clusters towards fragmentation must be due to the ability of the empty d orbitals of lanthanum to participate in the bonding to the carbon cluster. Thus inefficient formation of fullerenes containing late transition metals is due not only to the weakness of the endohedral complex, but also to the inability of the metals to bond strongly to the intermediates during the fullerene formation process.

$La_2C_n^+$ clusters

The results presented above for LaC_n^+, NbC_n^+ and PdC_n^+ clusters show that the isomers present are similar to those found for pure carbon clusters: rings, graphite fragments and fullerenes. There are, of course, important differences, which can be traced to the different electronic properties of the metal. Studies of metal-containing carbon clusters with substantially more than one metal atom have revealed the presence of exotic species such as metallocarbohedranes (clusters of the general formula M_8C_{12}), at least in the gas phase. Here, we consider the consequences of adding a second La atom to LaC_n^+ clusters.[29] Will the presence of the second metal atom cause the geometries to change dramatically?

Fig. 10 shows drift-time distributions recorded for unannealed and annealed $La_2C_{26}^+$, $La_2C_{28}^+$, $La_2C_{32}^+$, $La_2C_{48}^+$, $La_2C_{64}^+$ and $La_2C_{80}^+$. The isomers observed in the unannealed distributions fall into four families labelled: rings, full I, full + ring and full II. Only one isomer (labelled rings in Fig. 10) is observed for $La_2C_n^+$ ($n < 28$) clusters, while three (mono- and bi-cyclic rings and graphite sheets) are observed in this size range for MC_n^+ clusters [see Fig. 2(*c*)]. As we will describe below, the ring isomers are probably three-dimensional complexes of metal-containing carbon rings. These complexes appear to be stable and do not isomerize into planar rings when collisionally heated [compare Fig. 10(*a*) and 10(*b*)]. The rings feature is sharp for small clusters, but becomes increasingly broader for the larger ones. A fullerene isomer (labelled full I) first appears at $La_2C_{28}^+$. Fullerenes from the full I family have at least one non-endohedral metal atom (see below). Three-dimensional ring complexes with more than 30 carbon atoms isomerize into these fullerene isomers with increasing efficiency [see Fig. 10(*c*)–10(*h*)]. For $La_2C_n^+$ ($n > 45$) clusters the full I feature becomes broader and no longer corresponds to a single fullerene isomer. This broad feature (labelled full + ring or f + r in Fig. 10) is attributed to complexes of fullerenes and rings. These complexes readily convert into regular fullerenes upon collisional heating. Finally, a sharp full II peak, assigned to diendohedral fullerenes (see below), gradually appears in the drift-time distributions starting at $La_2C_{64}^+$ [see Fig. 10(*k*)]. For clusters larger than $La_2C_{80}^+$, the broad rings and full + ring features anneal predominantly into the diendohedral fullerene [see Fig. 10(*k*) and 10(*l*)].

Fig. 11 shows a plot of the inverse mobilities of the ring

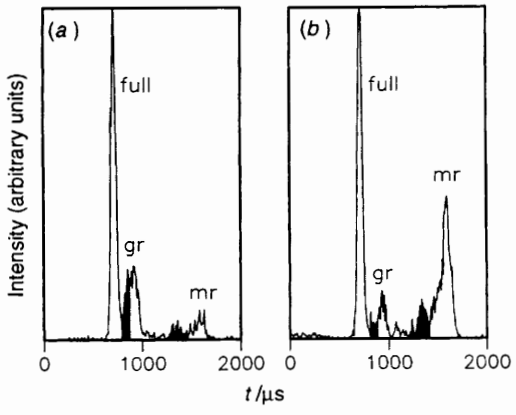

Fig. 9 Drift-time distributions for the C_{50}^+ product resulting from injection of PdC_{50}^+ into the drift tube at (*a*) 120 and (*b*) 200 eV

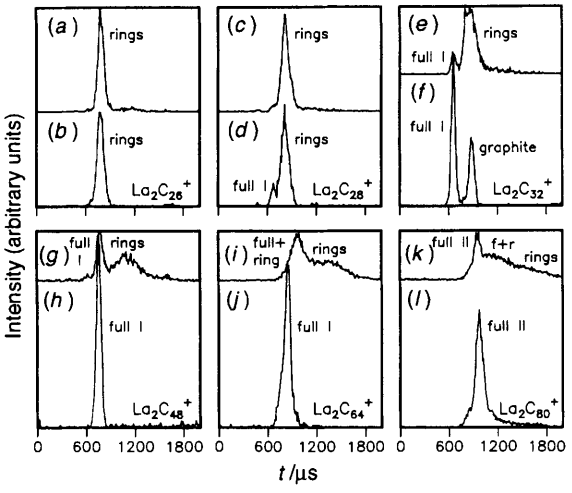

Fig. 10 Unannealed and annealed drift-time distributions recorded for $La_2C_{26}^+$, $La_2C_{28}^+$, $La_2C_{32}^+$, $La_2C_{48}^+$, $La_2C_{64}^+$ and $La_2C_{80}^+$. The injection energies were: 50 [(*a*), (*c*), (*e*), (*g*), (*i*) and (*k*)], 200 [(*d*)] 250 [(*b*) and (*f*)] and 300 eV [(*h*), (*j*) and (*l*)]. Shoulders at shorter drift times on the fullerene peaks in (*j*) and (*l*) are due to contaminants; f + r stands for fullerene + ring (see text)

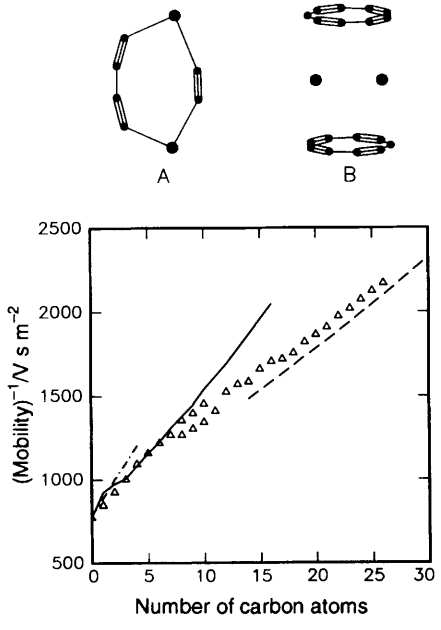

Fig. 11 Plots of the inverse mobilities of the $La_2C_n^+$ ring isomers. The measured mobilities are shown by △, while the lines show mobilities calculated for structures **A** (——), **B** (– – –) and for a linear chain (– · –)

isomers for clusters with up to 26 carbon atoms. The measured inverse mobilities are compared to inverse mobilities for several plausible geometries. For clusters with less than around 10 carbon atoms the measured inverse mobilities are close to those expected for a monocyclic ring where both lanthanum atoms are part of the ring. In this type of ring we expect that electrostatic interactions will drive the lanthanum atoms to be spaced as far apart as possible around the ring, as in structure **A** in the figure. For clusters with more than around 10 atoms the measured inverse mobilities increase less rapidly than the inverse mobilities predicted for the planar monocyclic rings. This observation suggests that the $La_2C_n^+$ ring isomers in this size range are three dimensional, in contrast to the roughly planar ring isomers observed for the MC_n^+ clusters. A three-dimensional complex of two metal-co-ordinated rings (such as structure **B** in Fig. 11) seems to be the most plausible structure for the larger $La_2C_n^+$ rings.

For LaC_n^+ fullerenes we have seen that the metal atom becomes endohedral as soon as it will fit. Where will the second metal atom go in $La_2C_n^+$ fullerenes?[30] The inverse mobilities of the $La_2C_n^+$ fullerene isomers are plotted in Fig. 12. The data were recorded with the drift tube at 80 K. As will become apparent below, multiple fullerene isomers are observed for the larger $La_2C_n^+$ clusters, and the lower drift-tube temperature permits a partial resolution of these isomers. The solid line in the figure shows the inverse mobilities of the smaller LaC_n^+ fullerenes, where the cage is too small to accommodate the lanthanum atom. The inverse mobilities of $La_2C_n^+$ (n = 28–30) are substantially larger than those of their LaC_n^+ analogues, suggesting that $La_2C_n^+$ (n = 28–30) fullerenes have two non-endohedral metal atoms. There is an abrupt decrease in the inverse mobilities of the $La_2C_n^+$ fullerenes at n = 31, and for n > 31 the $La_2C_n^+$ inverse mobilities are similar to those for the non-endohedral LaC_n^+ fullerenes. These results suggest that the first metal atom goes inside the cage at around n = 30 or 31. This is smaller than observed for LaC_n^+ clusters, where the metal goes inside for n = 34–37. Taken together, these results suggest that the non-endohedral lanthanum atom in small $La_2C_n^+$ fullerenes occupies a position in the cage, where it expands the cage and can stabilize an endohedral metal atom. Thus an endohedral metal atom can exist for smaller $La_2C_n^+$ fullerenes than for LaC_n^+ fullerenes.

For 64 carbon atoms there is a second distinct decrease in the inverse mobilities of the $La_2C_n^+$ fullerenes (see Fig. 12). This is the point where the cage becomes large enough to accommodate both metal atoms, and some of the larger fullerenes have two endohedral lanthanum atoms. The size of the smallest diendohedral metallofullerene we observe ($La_2C_{64}^+$) is close to that determined from laser 'shrink-wrapping' experiments.[31] In the 31–63 atom size range there is one endohedral and one non-endohedral metal atom. As can be seen from the figure, there are small odd–even oscillations in the inverse mobilities in this size range. These suggest that $La_2C_n^+$ fullerenes with an odd number of carbon atoms have a networked geometry (where one metal atom is part of the cage), and the even-numbered ones have an exohedral geometry (where the metal atom sits outside of a closed carbon cage). For clusters with more than 63 carbon atoms both metal atoms can fit inside the carbon cage. However, the diendohedral isomer is only observed for fullerenes with an even number of carbon atoms. The odd-numbered ones have one metal inside and one metal outside, probably in the carbon network. Thus the second lanthanum atom in $La_2C_n^+$ fullerenes appears to be behaving like the niobium atom in NbC_n^+ fullerenes. For the larger even-numbered $La_2C_n^+$ fullerenes the diendohedral isomer is not the only fullerene isomer present. There is also a significant amount of the isomer with one metal inside and one metal outside the cage. Even for the largest clusters studied, the relative abundance of the diendohedral isomer does not exceed 70–75%. Clearly, the forces driving the second lanthanum to become endohedral are much smaller than for the first. The electrostatic repulsion between the endohedral metal atoms, both of which are expected to donate significant electron density to the carbon cage, is the most likely reason for the observed behaviour. The reduced efficiency for encapsulating the second lanthanum could also result from stabilization of the non-endohedral geometries by the endohedral lanthanum atom.

Conclusion

We have described here the first systematic study of the structures and properties of metal-containing carbon clusters. While results are still only available for a fraction of the large number of possible metals and stoichiometries, some general conclusions can be drawn. Three basic types of geometry are observed for clusters with low metal/carbon ratios: rings, graphite fragments and fullerenes. However, the nature of these isomers depends on the electronic properties of the metal, and the number of metal atoms. Thus different types of ring

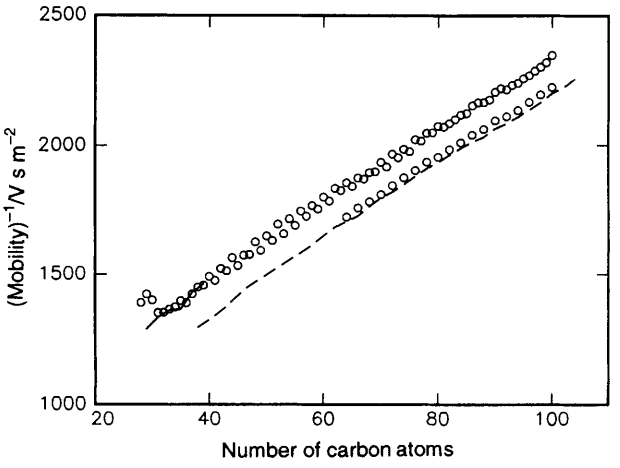

Fig. 12 Plots of the inverse mobilities of the $La_2C_n^+$ fullerene isomers. The lines show the inverse mobilities for pure C_n^+ fullerenes (– – –) and non-endohedral LaC_n^+ fullerenes (——). The inverse mobilities were measured with the drift tube at 80 K

isomers are observed for the different metals, and the ring isomers have different properties, for example some of the bicyclic rings isomerize into monocyclic rings while others do not. As the number of metal atoms increases the rings change from being roughly planar to three-dimensional structures that are probably complexes of rings. Metallofullerenes are only observed for early transition metals. The location of the metal (inside, outside or part of the carbon shell) also depends on its electronic properties. Early transition metals with low ionization energies form endohedral complexes, while transition metals from nearer the middle of the Periodic Table, with higher ionization energies and more valence electrons, also form a networked isomer. Endohedral or networked metallofullerenes are not observed for the late transition metals. When more than one metal atom is present the tendency to encapsulate a second metal atom is much smaller than for the first, presumably because of less favourable electrostatic interactions. The annealing studies provide insight into how the various isomers are assembled. The ring isomers for the early transition metals isomerize into metallofullerenes. The presence of the metal atom appears to promote this isomerization process because fullerene formation is much more efficient in the metal-containing carbon clusters than in the pure carbon analogues. For palladium, a late transition metal, metallofullerene formation was not observed. The metal atom appears to drop off during the isomerization process, leaving behind a pure carbon fullerene.

Acknowledgements

We gratefully acknowledge support of this work by the National Science Foundation (Grant No. CHE-9306900) and the Petroleum Research Fund (administered by the American Chemical Society).

References

1 L. Brus, *J. Phys. Chem.*, 1986, **90**, 2555.
2 J. L. Martins, R. Carr and J. Buttet, *Surf. Sci.*, 1981, **106**, 265, M. L. Cohen, M. Y. Chou, W. D. Knight and W. A. de Heer, *J. Chem. Phys.*, 1987, **91**, 3141.
3 H. W. Kroto, J. R. Heath, S. C. O'Brien, R. F. Curl and R. E. Smalley, *Nature (London)*, 1985, **318**, 162.
4 D. S. Bethune, R. D. Johnson, J. R. Salem, M. S. de Vries and C. S. Yannoni, *Nature (London)*, 1993, **366**, 123.
5 S. Wei, B. C. Guo, J. Purnell, S. Buzza and A. W. Castleman, *Science*, 1992, **255**, 818.
6 J. S. Pilgrim, L. R. Brock and M. A. Duncan, *J. Phys. Chem.*, 1995, **99**, 544.
7 D. F. Hagen, *Anal. Chem.*, 1979, **51**, 870; J. C. Tou and G. U. Boggs, *Anal. Chem.*, 1976, **48**, 1351; T. W. Carr, *J. Chromatogr.*, 1977, **15**, 85; Z. Karpas, M. J. Cohen, R. M. Stimac and R. F. Wernlung, *Int. J. Mass Spectrom. Ion Processes*, 1986, **83**, 163; R. H. St. Louis and H. H. Hill, *Crit. Rev. Anal. Chem.*, 1990, **21**, 321; G. von Helden, M. T. Hsu, P. R. Kemper and M. T. Bowers, *J. Chem. Phys.*, 1991, **95**, 3835.
8 M. F. Jarrold and V. A. Constant, *Phys. Rev. Lett.*, 1992, **67**, 2994.
9 G. von Helden, M.-T. Hsu, N. Gotts and M. T. Bowers, *J. Phys. Chem.*, 1993, **97**, 8192.
10 M. F. Jarrold, J. E. Bower and K. Creegan, *J. Chem. Phys.*, 1989, **90**, 3615; M. F. Jarrold and J. E. Bower, *J. Chem. Phys.*, 1992, **96**, 9180.
11 K. B. Shelimov, D. E. Clemmer and M. F. Jarrold, *J. Phys. Chem.*, 1995, **99**, 11386.
12 K. B. Shelimov, J. M. Hunter and M. F. Jarrold, *Int. J. Mass Spectrom. Ion Processes*, 1994, **138**, 17.
13 E. A. Mason and E. W. McDaniel, *Transport Properties of Ions in Gases*, Wiley, New York, 1988.
14 D. E. Clemmer, K. B. Shelimov and M. F. Jarrold, *J. Am. Chem. Soc.*, 1994, **116**, 5971.
15 M. Feyereisen, M. Gutowski and J. Simons, *J. Chem. Phys.*, 1992, **96**, 2926.
16 S. Yang, K. J. Taylor, M. J. Craycraft, J. Conceicao, C. L. Pettiette, O. Cheshnovsky and R. E. Smalley, *Chem. Phys. Lett.*, 1988, **144**, 431.
17 J. M. Hunter, J. L. Fye and M. F. Jarrold, *Science*, 1993, **260**, 784; G. von Helden, N. G. Gotts and M. T. Bowers, *Nature (London)*, 1993, **363**, 60.
18 D. E. Clemmer, K. B. Shelimov and M. F. Jarrold, *Nature (London)*, 1994, **367**, 718.
19 D. E. Clemmer and M. F. Jarrold, *J. Am. Chem. Soc.*, 1995, **117**, 10317.
20 D. E. Clemmer, J. M. Hunter, K. B. Shelimov and M. F. Jarrold, *Nature (London)*, 1994, **372**, 248.
21 K. Laasonen, W. Andreoni and M. Parrinello, *Science*, 1992, **258**, 1916; S. Nagase, K. Kobayashi, T. Kato and Y. Achiba, *Chem. Phys. Lett.*, 1993, **201**, 475.
22 P. B. Armentrout and R. Georgiadis, *Polyhedron*, 1988, **7**, 1573.
23 *CRC Handbook of Chemistry and Physics*, 63rd edn., ed. R. C. Weast, CRC Press, Boca Raton, FL, 1982.
24 T. Guo, R. E. Smalley and G. E. Scuseria, *J. Chem. Phys.*, 1993, **99**, 352.
25 K. B. Shelimov and M. F. Jarrold, unpublished work.
26 K. B. Shelimov and M. F. Jarrold, *J. Phys. Chem.*, 1995, **99**, 17677.
27 L. S. Sunderlin and P. B. Armentrout, *J. Am. Chem. Soc.*, 1989, **111**, 3845.
28 M. L. Mandich, L. F. Halle and J. L. Beauchamp, *J. Am. Chem. Soc.*, 1984, **106**, 4403.
29 K. B. Shelimov and M. F. Jarrold, *J. Am. Chem. Soc.*, in the press.
30 K. B. Shelimov and M. F. Jarrold, *J. Am. Chem. Soc.*, 1995, **117**, 6404.
31 Y. Chai, T. Guo, C. Jin, R. E. Haufler, L. P. F. Chibante, J. Fure, L. Wang, J. M. Alford and R. E. Smalley, *J. Phys. Chem.*, 1991, **95**, 7564.

Received 8th September 1995; *Paper* 5/06727H